

Morphological changes in polycrystalline Fe after compression and release

Nina Gunkelmann, Diego R. Tramontina, Eduardo M. Bringa, and Herbert M. Urbassek

Citation: *Journal of Applied Physics* **117**, 085901 (2015); doi: 10.1063/1.4913622

View online: <http://dx.doi.org/10.1063/1.4913622>

View Table of Contents: <http://scitation.aip.org/content/aip/journal/jap/117/8?ver=pdfcov>

Published by the [AIP Publishing](#)

Articles you may be interested in

[Clamping-induced changes of domain morphology in 88%Pb\(Zn_{1/3}Nb_{2/3}\)O₃-12%PbTiO₃](#)

J. Appl. Phys. **116**, 066812 (2014); 10.1063/1.4891312

[The interface and surface effects of the bicrystal nanowires on their mechanical behaviors under uniaxial stretching](#)

J. Appl. Phys. **108**, 074311 (2010); 10.1063/1.3477323

[Deformation twinning in nanocrystalline copper at room temperature and low strain rate](#)

Appl. Phys. Lett. **84**, 592 (2004); 10.1063/1.1644051

[Elastic and anelastic properties of Fe-doped InP films on silicon cantilevers](#)

J. Appl. Phys. **91**, 9031 (2002); 10.1063/1.1471921




[On a Simple Model Explaining the Hardening Effect in Poly-Crystalline Metals](#)

J. Rheol. **3**, 30 (1932); 10.1122/1.2116436



AIP | Journal of Applied Physics

Meet The New Deputy Editors

	Christian Brosseau		Laurie McNeil		Simon Phillpot
---	---------------------------	---	----------------------	---	-----------------------

Morphological changes in polycrystalline Fe after compression and release

Nina Gunkelmann,^{1,a)} Diego R. Tramontina,^{2,3,4} Eduardo M. Bringa,^{2,3}
 and Herbert M. Urbassek¹

¹Physics Department and Research Center OPTIMAS, University Kaiserslautern, Erwin-Schrödinger-Straße,
 D-67663 Kaiserslautern, Germany

²Instituto de Ciencias Básicas, Universidad Nacional de Cuyo, Mendoza 5500, Argentina

³CONICET, Mendoza 5500, Argentina

⁴Instituto de Bioingeniería, Universidad de Mendoza, Mendoza M5502BZ, Argentina

(Received 19 November 2014; accepted 15 February 2015; published online 25 February 2015)

Despite a number of large-scale molecular dynamics simulations of shock compressed iron, the morphological properties of simulated recovered samples are still unexplored. Key questions remain open in this area, including the role of dislocation motion and deformation twinning in shear stress release. In this study, we present simulations of homogeneous uniaxial compression and recovery of large polycrystalline iron samples. Our results reveal significant recovery of the body-centered cubic grains with some deformation twinning driven by shear stress, in agreement with experimental results by Wang *et al.* [Sci. Rep. **3**, 1086 (2013)]. The twin fraction agrees reasonably well with a semi-analytical model which assumes a critical shear stress for twinning. On reloading, twins disappear and the material reaches a very low strength value. © 2015 AIP Publishing LLC. [<http://dx.doi.org/10.1063/1.4913622>]

I. INTRODUCTION

The study of metals under compression is of vital importance in the modern world for understanding geophysical and astronomical processes and for technological processes which improve material properties. In particular, the deformation behavior of iron has been studied extensively both in monocrystals^{1,2} as well as in polycrystals.³ Shock experiments^{4–6} show that Fe undergoes a structural phase transition going from the body-centered cubic (bcc) to a hexagonal close-packed (hcp) structure⁷ at a pressure which varies from 13 GPa to more than 30 GPa depending on the strain rate.^{8,9} This phase transition, which is usually preceded by plastic yielding, was recently examined in several simulation studies.^{10–13}

However, there are still important issues that are not covered in our current understanding of shocks in Fe, particularly the characteristics of the structural behavior of the recovered material. Many laser-shot samples are thin, and they are destroyed during loading, precluding subsequent electron microscopy studies of the recovered material.^{8,9} Using dynamic diffraction, it was shown that shocked Fe single crystals transform to hcp nanocrystals during loading,¹⁴ but revert to single-crystal bcc after unloading,^{15–18} pointing to the large reversibility of the transformation path. The presence of grain boundaries (GB) in a polycrystal might, however, preclude such reversibility. GBs will limit the applicability of dynamic diffraction to check on reversibility, given that this method will typically average over thousands of grains in the sample. Indeed, a recent study on shocked Fe polycrystals, with a grain size in the region of tens of microns, reveals large amounts of twinning in recovered

samples,¹⁹ proposing a twinning path with shear and shuffle of atoms to explain the results.

In the present paper, we study homogeneous uniaxial compression and recovery of large polycrystalline iron samples. To this end, in Sec. III A, we analyze the stress-strain and heating behavior. The dislocation and twinning evolution are described in Sec. III B. Nearly perfect reversibility to the original bcc grains is achieved in our simulations with a limited presence of twinning. We are able to compare our results to the experiments by Wang *et al.*¹⁹ and to a constitutive twinning model described previously in the literature.²⁰

II. SIMULATION METHOD

The molecular dynamics (MD) code LAMMPS (Ref. 21) was used in this study to perform the simulations. We use a recent embedded-atom method (EAM) potential, similar to the Ackland and Mendelev potential,^{22,23} but fitted specifically to provide the bcc-hcp phase transition at 13.75 GPa. This potential is described in Ref. 10. Note that the Ackland potential was not developed to describe the high-temperature γ phase, and the bcc structure is stable up to the melting point (at zero pressure).

Our cubic sample contains approximately 2 million atoms and has an edge length of 30 nm. Sixty-four crystal grains with a mean grain size of 7.5 nm are created using a Voronoi construction scheme.²⁴ To equilibrate our systems, we first applied an energy minimization using the conjugate gradient method, and then relaxed the sample using high-temperature annealing at 80% of the melting temperature. During high-temperature annealing, the average potential energy per atom decreased from -4.28 eV after energy minimization to -4.29 eV. The potential energy value of -4.56 eV published in our previous paper was erroneous.¹⁰

^{a)}Electronic address: nina@gunkelmann.de

There was no significant grain growth during our annealing lasting 100 ps.

Simulations were carried within the microcanonical ensemble to be able to observe plastic heating, by performing uniaxial compression along the z axis at a strain rate of 10^9 s^{-1} , under periodic boundary conditions, up to a final strain around 20%. After holding this strain for 10 ps at a constant pressure p_{zz} of around 80 GPa, we unloaded the sample by applying uniaxial tension at the same strain rate to achieve zero uniaxial stress. This is the condition typically achieved under unloading conditions, where typical samples maintain a residual strain. Then we continued unloading during an additional 80 ps to reach a region of tension which could be relevant to some unloading experiments.

We chose an initial temperature of 10 K to facilitate dislocation analysis. Samples were visualized using common-neighbor analysis (CNA)^{25,26} and adaptive common-neighbor analysis²⁷ within OVITO (Ref. 28). We also used the Crystal Analysis Tool (CAT),²⁷ which allows for strain and structure-type calculations, including twin detection.

III. RESULTS

A. Stress-strain and heating behavior

We use the von-Mises stress to describe the driving stress for plastic activity. Using the components p_{ij} of the stress tensor, it is defined as

$$\sigma_{\text{vM}} = \sqrt{\frac{1}{2} \left[(p_{xx} - p_{yy})^2 + (p_{xx} - p_{zz})^2 + (p_{zz} - p_{yy})^2 + 6 \cdot (p_{xy}^2 + p_{xz}^2 + p_{yz}^2) \right]}. \quad (1)$$

The stress-strain curves in nanocrystals are influenced by GB sliding as well as by dislocation activity. GB sliding is significant mostly for small grains, with grain sizes up to $\sim 15\text{--}20$ nm.²⁹ Bcc nanocrystals^{3,30–33} have been studied less than fcc nanocrystals and display dislocations and twins under high-strain-rate loading. Fig. 1(a) shows the stress along the loading direction. At $\sim 8\%$ strain, the pressure reaches ~ 15 GPa and the phase transformation begins leading to tremendous hardening. There is some hysteresis during unloading, but the stress during unloading matches the loading stress as the strain approaches zero.

Fig. 1(a) shows the diagonal stress components. The off-diagonal stress terms are always smaller than 0.5 GPa and are not shown. Fig. 1(a) shows no residual strain at $p_{zz} = 0$. This is remarkable, since in most cases, high deformation would lead to plasticity and a residual strain after unloading. There are similar results in experiments and simulations of nanocrystalline fcc samples.^{34,35} However, those fcc results were for small strain deformation with recovery related to partial dislocations which are not present in bcc materials. In our samples, due to the small grain size, there are not many dislocations produced, and this could contribute to the lack of residual strain. Future simulations with much larger grain sizes which might facilitate dislocation emission³³ might be able to clarify this point. Regarding plasticity in the transformed hcp phase, stacking faults (SFs) are reabsorbed by GBs, as it was mentioned regarding fcc nanocrystals, contributing to the almost complete recovery of the stress tensor.

Fig. 1(b) shows the von-Mises stress. There is a quasi-elastic regime up to about 3% strain. GB sliding and dislocation emission (starting at 3.2 GPa) leads to a maximum in the stress and subsequent plastic relaxation. There is a sharp drop at the same time that the longitudinal pressure rapidly increases, with hardening starting at about 12% strain. Unloading shows an even faster softening, due to the rapid back-transformation to bcc. There is hardening also during unloading.

The mean potential energy of the atoms, Fig. 1(c), shows a change of about 0.5%. This indicates that as expected from the lack of residual strain, recovery is extremely good, but it is not perfect due to some plasticity. In particular, plastic heating leads to a temperature increase as described below. It is difficult to identify the precise location of the phase transformation from bcc to hcp in the stress-strain curves because of the presence of plasticity. GB sliding and dislocation motion, together with the phase transformation, lead to plastic heating and the temperature only slightly decreases during unloading, with a kink in unloading at 5% related to the hcp-bcc back-transformation, Fig. 1(d). Note that the temperature increase of $\sim 200 \text{ K} \cong 0.025 \text{ eV}$ is similar to the increase in potential energy. The temperature increase is small and will not lead to thermally activated processes in the time scale of our simulation. We note that for the—widely used—Voter potential,³⁶ substantially larger temperature effects have been identified in compression simulations, and this would influence the resulting recovered microstructure.¹⁰

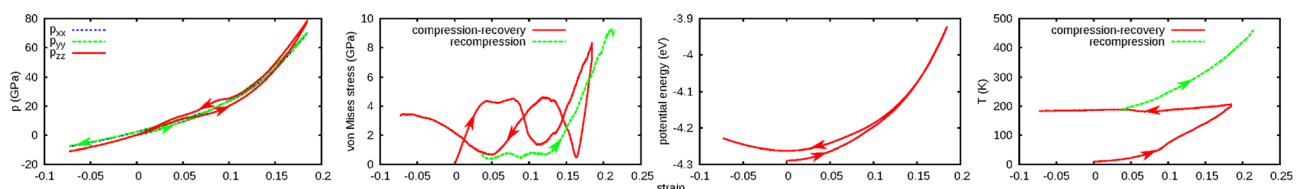


FIG. 1. Evolution of the sample during uniaxial compression, recovery, and recompression versus strain. (a) Diagonal stress components, (b) von-Mises stress, (c) potential energy, and (d) temperature versus strain. Loading/unloading is denoted by arrows on the curves.

The loading shown in Fig. 1 produces a complex microstructure, including recovery twins, as it will be shown in detail below. Twinning has been repeatedly related to improved mechanical properties.³⁷ Deformation twins are often found in samples recovered from high-strain-rate deformation experiments.^{38–41} In the last decade, nanoscale twinning in fcc metals has been shown to improve strength without impacting on other properties like conductivity, based on experiments and simulations.^{19,42,43} However, there are not as many studies on twinning for bcc metals,^{32,44–46} nor hcp metals,⁴⁷ especially at the nanoscale.

To study the possible change in material properties due to twinning in our nanocrystalline Fe samples, we recompressed the samples. One could expect improved hardness as in twinned fcc metals.⁴² The relatively small amount of twinning in our simulations is not expected to have a large impact on mechanical properties, but in contrast to what happens in fcc samples with twins, the stress-strain curves in Fig. 1(b) reveal a von-Mises stress which is low nearly up to 12% strain, with hardening at larger strains behaving nearly the same way as in the original sample. This will be analyzed in more detail below, but we note that the recompressed sample is at a slightly higher temperature, but in this case, temperature should not play a major role in dislocation motion and activation, and would modify GB sliding only slightly.³³

B. Dislocation activity and deformation twinning

Twinning simulations for bcc metals are challenging,⁴⁸ and twin identification in highly strained bcc metals is

complex.⁴⁹ We have used the adaptive common-neighbor analysis and the CAT (Ref. 27) to identify defects and phase-transformed material from our uniaxial compression and recovery. CAT is able to detect twins up to high strains.

At a strain of 15%, the material is almost fully transformed to a mixture of hcp and fcc, where the fcc phase appears mainly as stacking faults, as displayed in Fig. 2.

The results for the compression are identical to a previous study¹⁰ where we showed that dislocations emerge just before the phase transition starts, with several mixed dislocations showing fast edge segments which leave behind straight screw segments. The main reason for the shear stress drop in Fig. 1(b) is the phase transition, and then hardening occurs in the close-packed phase with production of SFs inside the hcp grains.

Unloading leads to a bcc nanocrystal. At a strain of 3%, near zero stress, the material is almost fully back-transformed to the bcc structure revealing several morphological features, including defects and twinning. Unloading twins nucleate from GBs, as discussed by Christian and Mahajan,³⁷ and shown for nanocrystalline bcc Ta during loading.³³ Twin boundaries appear as thin needle-like structures similar to experimental observations in polycrystalline iron.¹⁹ Note that we only consider bcc twins in our study to compare our results with these experiments¹⁹ and ignore the formation of twins in the newly formed hcp phase. In agreement with their results, twins appear as a result of the shear developing during the reverse phase transition from hcp to bcc. We find that twins appear in the $(\bar{1}21)[11\bar{1}]$ system, typical of bcc twins.⁵⁰

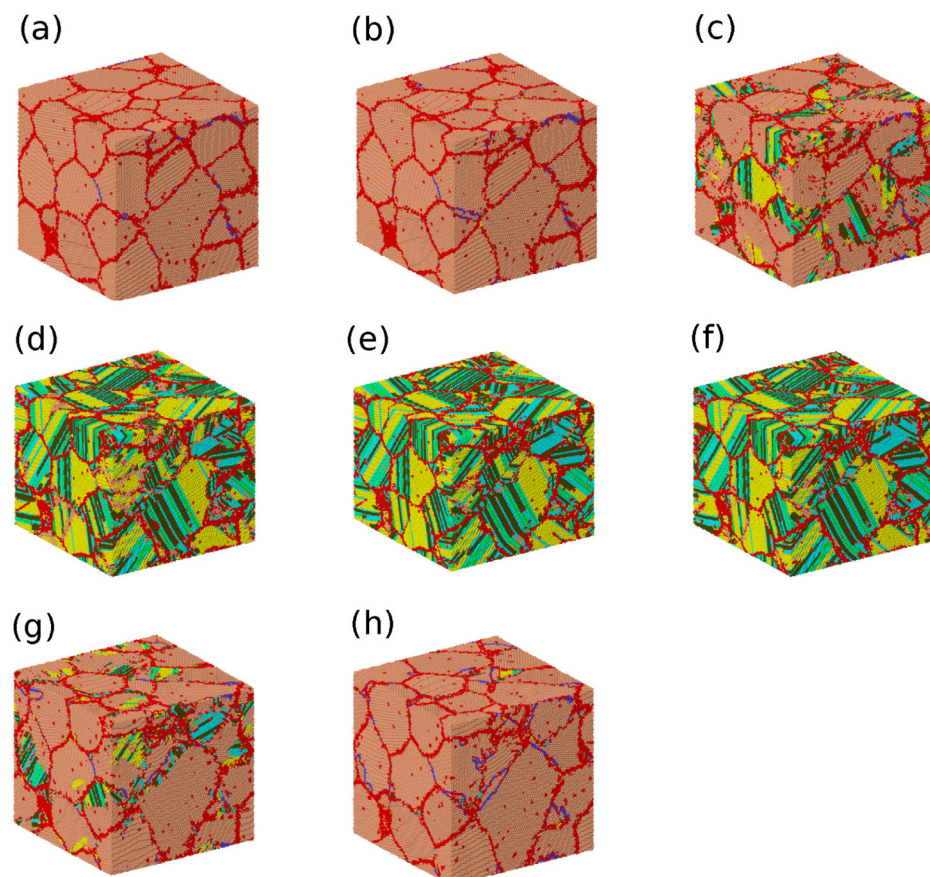


FIG. 2. Snapshots of the sample. Local atomic structures are identified by adaptive CNA and CAT.²⁷ Pink: bcc; red: bcc vacancies and intergranular atoms; yellow: hcp; teal: fcc; blue: bcc twin boundary. (a) 0%, (b) 5%, (c) 10%, (d) 15%, (e) 20% strain (loading), (f) 15%, (g) 4%, and (h) 0% strain (unloading).

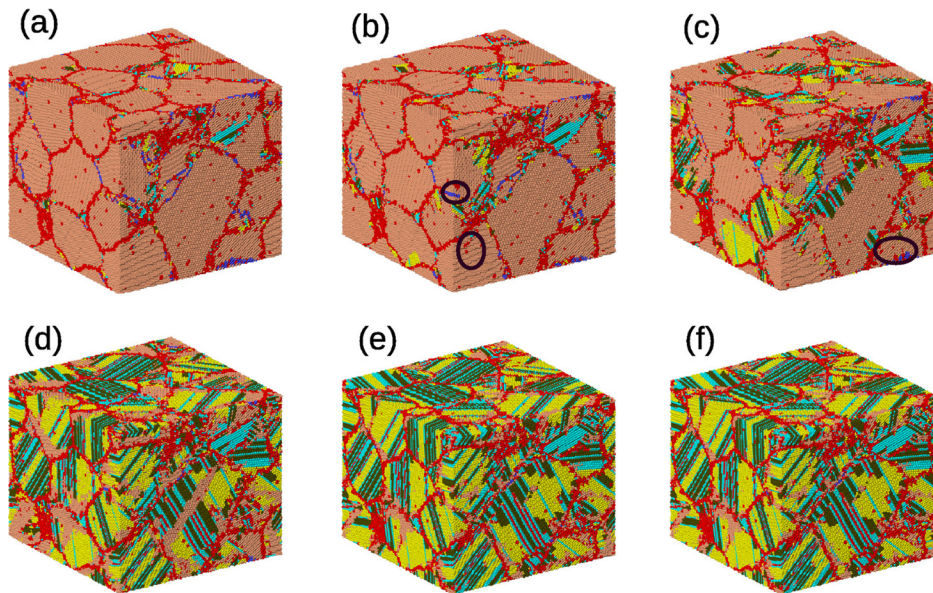


FIG. 3. Snapshots of the recompressed sample. (a) 0%, (b) 3%, (c) 5%, (d) 7%, (e) 9%, (f) 11% strain. Strain values are given with respect to the unloaded state at zero stress. Circles highlight dislocations. Color code denotes local atom structure as in Fig. 2.

Note that the grain topology in the back-transformed sample in Fig. 2(h) is the same as in the original sample, Fig. 2(a). GB free volume and GB sliding are sufficient to accommodate the transformation process without distorting the relative grain-grain orientations. This is consistent with the lack of residual strain and the small final change in potential energy, see Fig. 1(c). This is also consistent with the back-transformation to a single crystal observed in experiments and simulations.^{15–18}

Fig. 3 shows snapshots of the recompressed sample. A few dislocations—marked by circles—can be seen around 3–5% strain before the phase transition from bcc to hcp takes place. However, the recovered nanocrystal has experienced significant relaxation compared to the original crystal, and is able to deform with very low shear stress. Twins disappear during recompression and at 10% strain, the material is fully transformed to the hcp phase. Stacking faults in the hcp phase represent a finite amount of fcc phase as observed in the compression of the initial sample. This is the reason why hardening occurs similarly to the case of initial compression.

To give a more detailed description of twin formation, we analyzed the atomic motion during the bcc-hcp-bcc phase transition. To this end, Fig. 4 shows the displacement path of a small set of atoms within a twin structure after recovery. The hcp phase forms by compression of the $[00\bar{1}]_{\text{bcc}}$ axis, see Fig. 4(b), accompanied by atomic displacements. In Fig. 4(c), the atoms are sheared either along $[2\bar{1}\bar{1}0]_{\text{hcp}}$ or $[\bar{2}110]_{\text{hcp}}$ resulting in bcc twins. This process is similar to the shear-shuffle mechanism proposed by Wang *et al.*,¹⁹ where shearing takes place along $[11\bar{2}0]_{\text{hcp}}$ or $[\bar{1}\bar{1}20]_{\text{hcp}}$ resulting in bcc lattices with $(\bar{1}12)_{\text{bcc}}$ twinned relationship. The twins display three-fold-symmetry, strongly indicating that they arise from the intermediate hcp-phase which also has this symmetry.¹⁹ Recently, non-equilibrium MD simulations of shocks in single crystals using a Modified Analytic EAM potential (MAEAM) were performed,¹³ and a similar bcc-hcp transformation path was found; in addition, they analyzed ramp compression of single crystals with a similar result.¹¹

Fig. 5(a) shows the evolution of the phases analyzed by CAT.²⁷ As expected, we observe a steady decrease in the

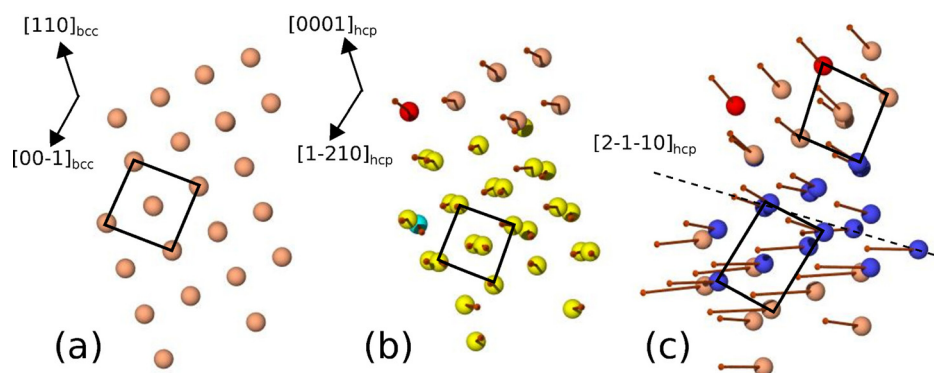


FIG. 4. Transformation path of the bcc-hcp-bcc phase transition. The $(100)_{\text{bcc}}$ plane corresponding to $(11\bar{2}0)_{\text{hcp}}$ is in the plane of the paper. Snapshots show selected atoms belonging to a twin at (a) 0 ps, at (b) 320 ps during the back-transformation of the hcp phase, and at (c) 360 ps after the back-transformation to the bcc phase; in the last stage, a twin boundary (highlighted in blue) has formed. Arrows denote the displacement of the atoms with respect to the initial configuration. Squares denote the unit cells of the bcc phase which is deformed during the process. Atoms are compressed along the $[00\bar{1}]_{\text{bcc}}$ axis to create the hcp primitive cell. During recovery, corresponding to (b), the atoms are sheared either along $(2\bar{1}\bar{1}0)_{\text{hcp}}$ or $[\bar{2}110]_{\text{hcp}}$ resulting in bcc twins of $(\bar{1}12)_{\text{bcc}}$ twin plane. Color code denotes local atom structure as in Fig. 2.

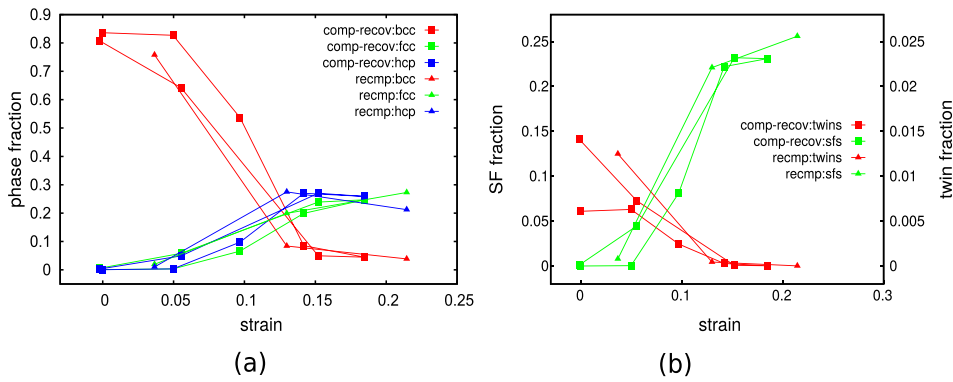


FIG. 5. Evolution of (a) phase fraction and (b) twin and stacking-fault (SF) fractions versus strain.

bcc phase with higher strain. The material transforms to close-packed phases, primarily to hcp, but there is also a finite amount of fcc. The evolution of the phases is mainly driven by strain so that the behavior is similar for loading, unloading, and recompression.

We define the twin fraction as the number of atoms forming twin boundaries with respect to the total number of atoms; and similarly the stacking-fault fraction as the relative number of atoms found in stacking-fault positions. It is difficult, for the large number of grains we use, to define a volumetric twin fraction, or an areal twin fraction for a given cross-section of the sample as often done in microscopy. Fig. 5(b) shows the twin fraction and the stacking-fault fraction versus strain for both compression, recovery and recompression.

We note that there is a finite bcc twin fraction even at zero strain before compression of the sample which decreases to nearly zero during the compression of the sample. However, these atoms identified as belonging to twin boundaries are actually part of the structure of some GBs in the initial GB network, as seen in Fig. 2(a).

We observe that the twin fraction inside the bcc grains increases during recovery while the amount of stacking faults decreases. Detailed inspection of the sample confirms that these are indeed twins. On reloading, these twins disappear; this fact suggests that twin formation/detwinning are driven by inversion of the shear stress. This is expected from the process of detwinning during unloading as reported for fcc materials,⁵¹ bcc nanowires,⁴⁶ and nanoindentation in Ta.⁴⁵ Since unloading occurs from a compressed state, there is no twin-induced GB cracking⁵² or cracking-induced twinning.³³

Fig. 6 presents the twin fraction as obtained by CAT from our simulations. We compare our results on twinning to a constitutive model that has been proposed by Johnson and Rohde,²⁰ including dislocation slip and deformation twinning. In this model, the volume fraction of twinned material results from the growth of pre-existing twin platelets via

$$\alpha = \left[\alpha_0^{1/m} + \frac{1}{t_m} \int_0^t v_m(\tau(t)) dt \right]^m, \quad (2)$$

where $\alpha_0 = 0.006$ is the initial fraction of twins, the exponent m assumes the value $m = 3$ for volumetric and $m = 2$ for areal growth, t_m is the characteristic time and v_m is the dimensionless growth rate increasing linearly with stress τ :

$$v_m(\tau) = \begin{cases} \frac{\tau}{\tau_0} - 1, & \tau \geq \tau_0, \\ 0, & \text{else,} \end{cases} \quad (3)$$

where τ_0 is the threshold stress for twinning. τ depends on time t during the compression and recovery phase. To define τ , we use here the shear stress often used for the analysis of shock simulations⁵³

$$\tau_{\text{shear}} = -\frac{1}{2} \left[p_{zz} - \frac{1}{2} (p_{xx} + p_{yy}) \right]. \quad (4)$$

It is similar to the von-Mises stress, Eq. (1), if off-diagonal terms are neglected, but it can assume positive or negative values, in this case depending on loading or unloading. As mentioned above, the non-diagonal stress components are small in all stages of our simulations.

Since the twin fraction we measure is related to twin boundary surface, we use the model, Eq. (2) with $m = 2$. The model by Johnson and Rohde²⁰ was developed for cases where twinning is driven by shear stress. In contrast, in our case, twinning is triggered by the phase transformation.

Equation (2) is solved using the trapezoidal integration rule.⁵⁴ Fig. 6 shows that the agreement between the model and our data is only mediocre. We therefore improve the model by assuming a simplified, constant twin growth above a threshold stress τ_d :

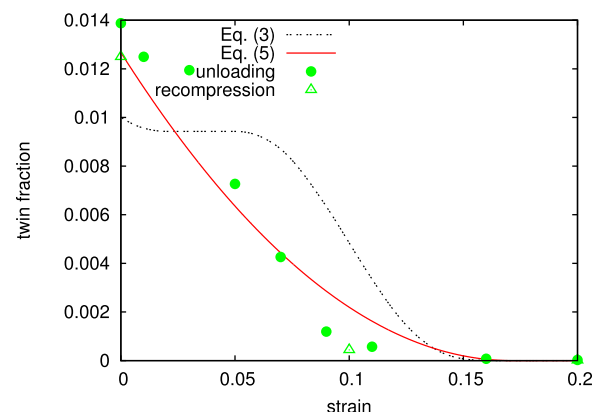


FIG. 6. Twin fraction as obtained by simulation (symbols) compared to an analytical model using two different growth models, Eqs. (3) and (5), versus strain.

$$v_m(\tau) = \begin{cases} a, & \tau \geq \tau_d, \\ -a, & \tau \leq -\tau_d \\ 0, & \text{else.} \end{cases} \quad (5)$$

Here, we also describe detwinning. We note that the model by Johnson and Rohde²⁰ was meant to fit twinning at much lower shock pressures and strain rates, for polycrystalline Fe samples with much larger grain sizes, and close agreement with our results should not be expected.

Similar to Ref. 55, we used the characteristic time t_m as fit parameter. By least-squares fitting, the best fit is $t_m = 3.5$ ns comparable to laser-shock experiments where the characteristic time of loading duration and unloading is in the order of 1 ns.⁵⁵ We fit also the threshold stress and the parameter a and obtain a best fit of $\tau_0 = 0.4$ GPa, $\tau_d = 0.1$ GPa, and $a = 2.3$.

Since the phase transformation helps to drive twinning, this threshold stresses are lower than shear values near 2 GPa for simulations of twinning in defective single crystals under shock loading⁵³ or homogeneous compressive loading.⁵⁶

The fitted threshold stress τ_0 is actually close to typical experimental values used for twinning in Fe and other bcc metals which are usually smaller than 0.5 GPa.^{38,55,57} Note, however, that in our simulation, we employ both higher strain rate and smaller grain sizes than in most experiments. High strain rate is not expected to increase the twinning threshold stress.⁵⁸ However, if one would consider a Hall-Petch (HP) type model for the influence of grain size on twinning,^{40,57,58} the threshold value should actually be much higher for our 7.5 nm grains; this can be shown as follows. Meyers *et al.*⁵⁷ derived an expression for the dependence of the threshold stress for twinning on the average grain size d :

$$\tau_0 = S_0 + kd^{-0.5}. \quad (6)$$

Inserting a value of $d = 7.5$ nm as applicable for our simulation and the constants $S_0 = 450$ MPa and $k = 100$ MPa mm^{0.5} for bcc iron,⁵⁷ Eq. (6) predicts $\tau_0 = 37$ GPa, which is considerably higher than our value of 0.4 GPa. This calculation demonstrates that the HP slopes from μm -sized grains are typically not applicable to nanoscale grains.⁵⁹

Fig. 6 presents the comparison between MD values and the constitutive relations from above, Eqs. (2)–(5). Note that the twin fraction is plotted versus strain instead of time because the quantities are proportional. The number of twins increases during the recovery of the sample with smaller strain values. Our model equation (5) and the measured values are in good agreement so that the twin fraction increases at a strain of 10% during unloading, coincident with the onset of the hcp-bcc back-transformation and decreases again during recompression. The agreement between the predicted values by Johnson and Rohde and the measured MD values is not convincing. We follow that the twin evolution is not driven by shear stress but depends mainly on the phase transformation. A further reason why the model might not offer good agreement with the MD results is that the scenario in our simulation is somewhat different from that studied in the model. In our case, twins are nucleated from GBs, and

then grow. There is no growth of a simple twin lamella isolated in a single-crystal matrix, as assumed in most models for twin growth like the one by Sandoval *et al.*⁶⁰ or the one by Florando *et al.*,⁴¹ which also incorporate dislocation-twin competition.⁴¹ In contrast, in our case, twins are generated due to the phase transition so that twin nucleation may be important, as in hcp metals.⁶¹ However, twin nucleation stress is small for bcc iron⁴⁶ and we only consider bcc twins in our study.

In our study, we find that the α - ϵ phase transformation exerts a decisive influence on the twinning and detwinning under compression and release. We performed an analogous simulation for our poly-crystalline specimen, where we used a potential which is very similar to the Ackland potential used up to now, but which does not allow for phase transformation.⁶² Then we find that the number of bcc twins *increases* under compression and *decreases* during release; in other words, the twin fraction simply increases with strain in the material. This behavior is totally different from our finding in Fig. 6. This comparison demonstrates that the possibility of phase transformation in real Fe is decisive for the morphological changes found.

IV. SUMMARY

We analyzed the response of polycrystalline α -iron to homogeneous uniaxial loading and unloading in order to describe the dislocation activity and deformation twinning in recovery simulations of high strain-rates. After recovery, nearly the same nanocrystal as before loading is re-established. This fact is supported by a negligibly small difference in average potential energy before compression and after recovery, and small plastic heating. Our result is also consistent with experiments for single-crystal Fe, where the single crystal is recovered despite the fact that a polycrystal was created during loading.^{15,17,18} This is consistent with the fact that twinning is reversed alongside with phase transformation. Even though we have violent events (phase transformation, plasticity), the original structure is preserved because twinning and detwinning are solely driven by the phase transformation.

Our analysis shows that recovery leads to twinning inside the recovered bcc grains.

The structure of the twins is in good agreement with the experimental results by Wang *et al.*,¹⁹ and the twin formation path also agrees with the one they proposed. On reloading, the twins disappear. The evolution of twins can be fairly described by a modified version of the constitutive model by Johnson and Rohde²⁰ and is driven by the phase transformation from bcc to hcp and vice-versa.

We note that in metals, shock-induced hardening is related to an increased dislocation density,³⁹ even for nanocrystals with a grain size of tens of nm.³⁴ Here the simulated grain size precludes significant dislocation storage, and hardening can be neglected. The lack of residual hardening, together with significant GB relaxation due to the back-transformation, leads to a recovered nanocrystal which has extremely low strength upon recompression. This complex scenario might also occur in experiments for small nanocrystals.

Future simulations will cover larger grain sizes, and non-equilibrium MD shock recovery simulations of nanocrystals, where the transient wave profile might change the unloaded microstructure.

ACKNOWLEDGMENTS

This work has been supported by the *Deutsche Forschungsgemeinschaft* via the Sonderforschungsbereich 926. Eduardo M. Bringa acknowledges support from CONICET, SeCTyP (U.N. Cuyo), and PICT-2009-0092. Simulations were performed at the High Performance Cluster Elwetritsch (Elwetritsch, RHRK, TU Kaiserslautern, Germany).

- ¹J. L. Shao, S. Q. Duan, A. M. He, C. S. Qin, and P. Wang, *J. Phys.: Condens. Matter* **21**, 245703 (2009).
- ²V. V. Stegailov and A. V. Yanilkin, *Sov. Phys. - JETP* **104**, 928 (2007).
- ³J. B. Jeon, B.-J. Lee, and Y. W. Chang, *Scr. Mater.* **64**, 494 (2011).
- ⁴J. C. Boettger and D. C. Wallace, *Phys. Rev. B* **55**, 2840 (1997).
- ⁵B. J. Jensen, G. T. Gray III, and R. S. Hixson, *J. Appl. Phys.* **105**, 103502 (2009).
- ⁶R. F. Smith, J. H. Eggert, R. E. Rudd, D. C. Swift, C. A. Bolme, and G. W. Collins, *J. Appl. Phys.* **110**, 123515 (2011).
- ⁷W. Pepperhoff and M. Acet, *Constitution and Magnetism of Iron and its Alloys* (Springer, Berlin, 2001).
- ⁸R. F. Smith, C. A. Bolme, D. J. Erskine, P. M. Celliers, S. Ali, J. H. Eggert, S. L. Brygoo, B. D. Hammel, J. Wang, and G. W. Collins, *J. Appl. Phys.* **114**, 133504 (2013).
- ⁹J. C. Crowhurst, B. W. Reed, M. R. Armstrong, H. B. Radousky, J. A. Carter, D. C. Swift, J. M. Zaug, R. W. Minich, N. E. Teslich, and M. Kumar, *J. Appl. Phys.* **115**, 113506 (2014).
- ¹⁰N. Gunkelmann, E. M. Bringa, K. Kang, G. J. Ackland, C. J. Ruestes, and H. M. Urbassek, *Phys. Rev. B* **86**, 144111 (2012).
- ¹¹K. Wang, S. Xiao, M. Liu, H. Deng, W. Zhu, and W. Hu, *Proc. Eng.* **61**, 122 (2013).
- ¹²N. Gunkelmann, E. M. Bringa, D. R. Tramontina, C. J. Ruestes, M. J. Suggit, A. Higginbotham, J. S. Wark, and H. M. Urbassek, *Phys. Rev. B* **89**, 140102 (2014).
- ¹³K. Wang, S. Xiao, H. Deng, W. Zhu, and W. Hu, *Int. J. Plast.* **59**, 180 (2014).
- ¹⁴J. A. Hawreliak, D. H. Kalantar, J. S. Stölken, B. A. Remington, H. E. Lorenzana, and J. S. Wark, *Phys. Rev. B* **78**, 220101 (2008).
- ¹⁵B. El-Dasher, W. MoberlyChan, J. McNaney, J. Hawreliak, and H. Lorenzana, in American Physical Society Meeting Abstracts L23.00003, Bulletin of the American Physical Society, 2007, Vol. 52.
- ¹⁶K. Kadau, T. C. Germann, P. S. Lomdahl, and B. L. Holian, *Phys. Rev. B* **72**, 064120 (2005).
- ¹⁷W. MoberlyChan, B. S. El-Dasher, and G. H. Campbell, *Microsc. Microanal.* **15**, 364 (2009).
- ¹⁸W. MoberlyChan, private communication (2014).
- ¹⁹S. J. Wang, M. L. Sui, Y. T. Chen, Q. H. Lu, E. Ma, X. Y. Pei, Q. Z. Li, and H. B. Hu, *Sci. Rep.* **3**, 1086 (2013).
- ²⁰J. N. Johnson and R. W. Rohde, *J. Appl. Phys.* **42**, 4171 (1971).
- ²¹S. Plimpton, *J. Comput. Phys.* **117**, 1 (1995).
- ²²M. I. Mendelev, S. Han, D. J. Srolovitz, G. J. Ackland, D. Y. Sun, and M. Asta, *Philos. Mag.* **83**, 3977 (2003).
- ²³G. J. Ackland, M. I. Mendelev, D. J. Srolovitz, S. Han, and A. V. Barashev, *J. Phys.: Condens. Matter* **16**, S2629 (2004).
- ²⁴A. Frøseth, H. Van Swygenhoven, and P. Derlet, *Acta Mater.* **53**, 4847 (2005).
- ²⁵D. Faken and H. Jonsson, *Comput. Mater. Sci.* **2**, 279 (1994).
- ²⁶H. Tsuzuki, P. S. Branicio, and J. P. Rinoi, *Comput. Phys. Commun.* **177**, 518 (2007).
- ²⁷A. Stukowski, *Modell. Simul. Mater. Sci. Eng.* **20**, 045021 (2012).
- ²⁸A. Stukowski and K. Albe, *Modell. Simul. Mater. Sci. Eng.* **18**, 085001 (2010).
- ²⁹M. A. Meyers, A. Mishra, and D. J. Benson, *Prog. Mater. Sci.* **51**, 427 (2006).
- ³⁰A. Latapie and D. Farkas, *Phys. Rev. B* **69**, 134110 (2004).
- ³¹D. Farkas and B. Hyde, *Nano Lett.* **5**, 2403 (2005).
- ³²R. E. Rudd, *Mater. Sci. Forum* **633–634**, 3 (2009).
- ³³Y. Tang, E. M. Bringa, and M. A. Meyers, *Mater. Sci. Eng., A* **580**, 414 (2013).
- ³⁴E. M. Bringa, A. Caro, Y. Wang, M. Victoria, J. M. McNaney, B. A. Remington, R. F. Smith, B. R. Torralva, and H. Van Swygenhoven, *Science* **309**, 1838 (2005).
- ³⁵Z. Budrovic, H. Van Swygenhoven, P. M. Derlet, S. Van Petegem, and B. Schmitt, *Science* **304**, 273 (2004).
- ³⁶R. J. Harrison, A. F. Voter, and S.-P. Chen, in *Atomistic Simulation of Materials: Beyond Pair Potentials*, edited by V. Vitek and D. J. Srolovitz (Plenum Press, New York, 1989), p. 219.
- ³⁷J. W. Christian and S. Mahajan, *Prog. Mater. Sci.* **39**, 1 (1995).
- ³⁸L. E. Murr, M. A. Meyers, C.-S. Niou, Y. J. Chen, S. Pappu, and C. Kennedy, *Acta Mater.* **45**, 157 (1997).
- ³⁹M. A. Meyers, H. Jarmakani, E. Bringa, and B. A. Remington, in *Dislocations in Solids*, edited by J. P. Hirth and L. Kubin (Elsevier, 2009), Vol. 13, Chap. 89, pp. 91–197.
- ⁴⁰C. H. Lu, B. A. Remington, B. R. Maddox, B. Kad, H. S. Park, S. T. Prisbrey, and M. A. Meyers, *Acta Mater.* **60**, 6601 (2012).
- ⁴¹J. N. Florando, N. R. Barton, B. S. El-Dasher, J. M. McNaney, and M. Kumar, *J. Appl. Phys.* **113**, 083522 (2013).
- ⁴²L. Lu, X. Chen, X. Huang, and K. Lu, *Science* **323**, 607 (2009).
- ⁴³K. Lu, L. Lu, and S. Suresh, *Science* **324**, 349 (2009).
- ⁴⁴Y. T. Zhu, X. Z. Liao, and X. L. Wu, *Prog. Mater. Sci.* **57**, 1 (2012).
- ⁴⁵C. J. Ruestes, A. Stukowski, Y. Tang, D. R. Tramontina, P. Erhart, B. A. Remington, H. M. Urbassek, M. A. Meyers, and E. M. Bringa, *Mater. Sci. Eng., A* **613**, 390 (2014).
- ⁴⁶A. Cao, *J. Appl. Phys.* **108**, 113531 (2010).
- ⁴⁷Q. Yu, L. Qi, K. Chen, R. K. Mishra, J. Li, and A. M. Minor, *Nano Lett.* **12**, 887 (2012).
- ⁴⁸R. Zhang, J. Wang, I. Beyerlein, and T. Germann, *Philos. Mag. Lett.* **91**, 731 (2011).
- ⁴⁹A. Higginbotham, M. J. Suggit, E. M. Bringa, P. Erhart, J. A. Hawreliak, G. Mogni, N. Park, B. A. Remington, and J. S. Wark, *Phys. Rev. B* **88**, 104105 (2013).
- ⁵⁰Y. Tang, E. M. Bringa, and M. A. Meyers, *Acta Mater.* **60**, 4856 (2012).
- ⁵¹C. J. Shute, B. D. Myers, S. Xie, S.-Y. Li, T. W. Barbee, Jr., A. M. Hodge, and J. R. Weertman, *Acta Mater.* **59**, 4569 (2011).
- ⁵²Y. Zhang, P. C. Millett, M. Tonks, and B. Biner, *Scr. Mater.* **66**, 117 (2012).
- ⁵³D. Tramontina, P. Erhart, T. Germann, J. Hawreliak, A. Higginbotham, N. Park, R. Ravelo, A. Stukowski, M. Suggit, Y. Tang *et al.*, *High Energy Density Phys.* **10**, 9 (2014).
- ⁵⁴R. L. Burden and J. D. Faires, *Numerical Analysis* (Thompson, 2005).
- ⁵⁵T. de Rességuier and M. Hallouin, *J. Appl. Phys.* **84**, 1932 (1998).
- ⁵⁶D. Tramontina, C. Ruestes, Y. Tang, and E. Bringa, *Comput. Mater. Sci.* **90**, 82 (2014).
- ⁵⁷M. A. Meyers, O. Vöhringer, and V. A. Lubarda, *Acta Mater.* **49**, 4025 (2001).
- ⁵⁸R. W. Armstrong, W. Arnold, and F. J. Zerilli, *J. Appl. Phys.* **105**, 023511 (2009).
- ⁵⁹S. D. Antolovich and R. W. Armstrong, *Prog. Mater. Sci.* **59**, 1 (2014).
- ⁶⁰L. A. Sandoval, M. P. Surh, A. A. Chernov, and D. F. Richards, *J. Appl. Phys.* **114**, 113511 (2013).
- ⁶¹X. Y. Lou, M. Li, R. K. Boger, S. R. Agnew, and R. H. Wagoner, *Int. J. Plast.* **23**, 44 (2007).
- ⁶²G. J. Ackland, D. J. Bacon, A. F. Calder, and T. Harry, *Philos. Mag.* **75**, 713 (1997).